# Experimental and Numerical Investigations of a Flexible Rotor on Flexible Bearing Supports

Jean-Jacques Sinou, Cristiano Villa, Fabrice Thouverez

International Journal of Rotating Machinery 2005:3, 179–189


# Experimental and Numerical Investigations of a Flexible Rotor on Flexible Bearing Supports

**J.-J. Sinou**

*Equipe Dynamique des Structures et des Systèmes, Laboratoire de Tribologie et Dynamique des Systèmes, UMR CNRS 5513, École Centrale de Lyon, Batiment E6, 36 avenue Guy de Collongue, 69134 Ecully Cedex, France*
*Email: jean-jacques.sinou@ec-lyon.fr*

**C. Villa**

*Equipe Dynamique des Structures et des Systèmes, Laboratoire de Tribologie et Dynamique des Systèmes, UMR CNRS 5513, École Centrale de Lyon, Batiment E6, 36 avenue Guy de Collongue, 69134 Ecully Cedex, France*
*Email: cristiano.villa@ec-lyon.fr*

**F. Thouverez**

*Equipe Dynamique des Structures et des Systèmes, Laboratoire de Tribologie et Dynamique des Systèmes, UMR CNRS 5513, École Centrale de Lyon, Batiment E6, 36 avenue Guy de Collongue, 69134 Ecully Cedex, France*
*Email: fabrice.thouverez@ec-lyon.fr*

*Received 30 August 2005*

The main goal of this paper is to study, numerically and experimentally, the effects of the bearing support flexibility on the rotor dynamic and the first forward and backward critical speeds. The test rig which is used in this study has been developed and built at the École Centrale de Lyon (France). This flexible rotor, supported by two rolling bearings on flexible supports, is used for three configurations of the flexible supports. The support characteristics are determined experimentally by performing static tests. Moreover, a finite element model of this flexible rotor is presented which consists of a rigid disk on a flexible shaft supported by two bearing supports. On the basis of measured frequency response functions for various rotational speeds, eigenfrequencies and the associated Campbell diagram from the numerical model and the related experimental results for the flexible rotor are discussed. The comparison of these experimental and numerical tests are used in order to update the finite element model and the associated moment stiffness of the two rolling bearings for the three configurations of interest.

**Keywords and phrases:** flexible rotor, experimental tests, finite element model, Campbell diagram, critical speed.

## 1. INTRODUCTION

Vibration of turbomachinery can very seriously affect theintegrity of industrial plants. Effectively, due to the fact that most of the rotating machinery operate above the first critical speed, it has become increasingly important over the past years to predict the dynamic behavior accurately. In fact, rotating motion, backward and forward critical speeds, and steady-stateresponse are design criteria of rotating machinery and play an important role in diagnosis and control of rotors.



During the past decades, the use of flexible supports was strongly developed due to some practical advantages offered by this design. A number of authors [1, 2, 3, 4, 5, 6, 7, 8, 9, 10, 11] have addressed this problem, highlighted the importance of this component, and triedto use experimental procedures and data in order to undertake the influence of the support flexibility of rotor machinery.

Effectively, the dynamic behavior of rotating machines may be drastically affected by the characteristics of the support flexibility of rotor machinery. Then, one of the main objectives of the researchers and designers was to be able to obtain fundamental mathematical models, adequate to the observed physical phenomena, in order to predict numerically the dynamic behavior of rotor systems and the influence of the support flexibility of rotors. In recent years,

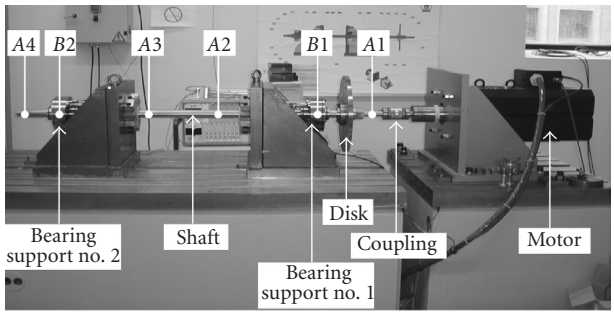


Figure 1: Description of the test rotor.

there has been an important research activity in the field of modeling and analysis of the dynamic behavior of rotating machinery in order to adjust some system parameters and to obtain the most suitable design within the speed range of interest. Then, the utilization of finite element models in the area of rotor dynamics was applied to develop suitable models and has yielded highly successful results [10, 11, 12, 13, 14, 15, 16, 17, 18]. These numerical models are now used to design machinery to operate within acceptable limits.

This paper will focus on experimental tests and the utilization of the finite element model in order to accommodate the effects of the support flexibility on the dynamic behavior of rotor systems. It will be demonstrated that the support flexibility of rotor machinery may have a significant effect on the machine dynamics and can be correctly predicted by using numerical models.

First of all, the flexible rotor developed at the Laboratoire de Tribologie et Dynamique des Systèmes UMR CNRS 5513 of the École Centrale de Lyon (France) and the associated finite element model are presented. Secondly, experimental tests based on the unbalance response, the Campbell diagram, and the orbits' evolutions are performed. Then the influence of the flexible support is investigated in order to be able to predict the variations of the first backward and forward critical speed of the flexible rotor. Finally, correlations between the experimental tests and the finite element model is carried out in order to update the numerical model. The comparisons between the experimental and numerical results are performed for the three configurations of the flexible rotor by considering more particularly the critical speed zones of interest.

## 2. DESCRIPTION OF THE TEST RIG

The investigated test rotor is composed of a horizontal flexible shaft of 1700 mm length with a circular cross-section of 40 mm as shown in Figure 1. The shaft is connected to an electricalmotor by a flexible coupling and has one disk of a diameter of 400 mm and a thickness of 20 mm attached at 196 mm to the end of the shaft that has the flexible coupling. This shaft is supported by two bearings and two

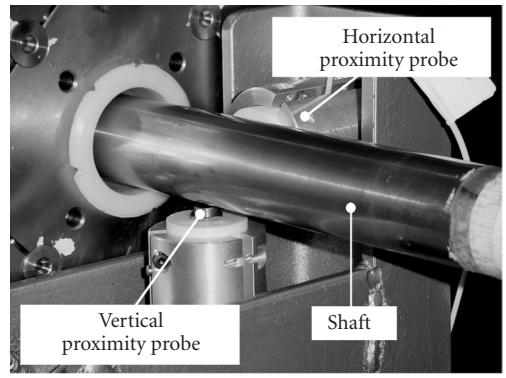


(a)

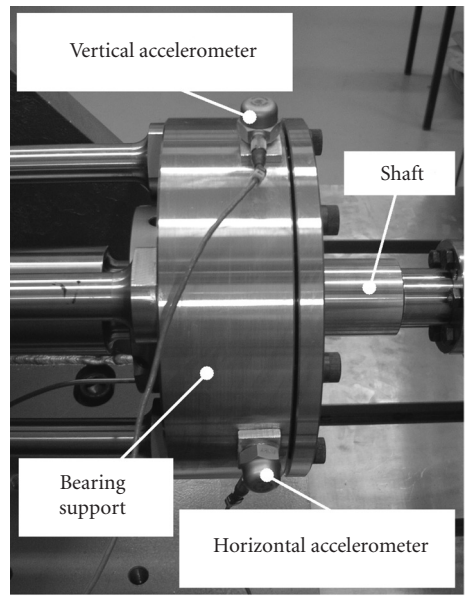


(b)

Figure 2: Detail of two planes of measures: (a) proximity probes and (b) accelerometers.

bearing supports; the two supports are placed at 342 mm and 1478 mm, respectively, from the end of the shaft that has the flexible coupling. The entire apparatus is clamped to a massive concrete block isolated from the environment by rubber pads.

Six stations of the rotor are measured simultaneously: eight noncontactdisplacement sensors consisting of two orthogonal sensors for each plane are placed at 10 mm (plane $A1$), 72 mm (plane $A2$), 108 mm (plane $A3$), and 164 mm (plane $A4$), respectively, from the end of the shaft that has the flexible coupling, as indicated in Figure 2a. Moreover, four accelerometers consisting of two orthogonal accelerometers for each plane are placed in the bearing supports, as shown in Figure 2b. The rotor has also a phase meter.

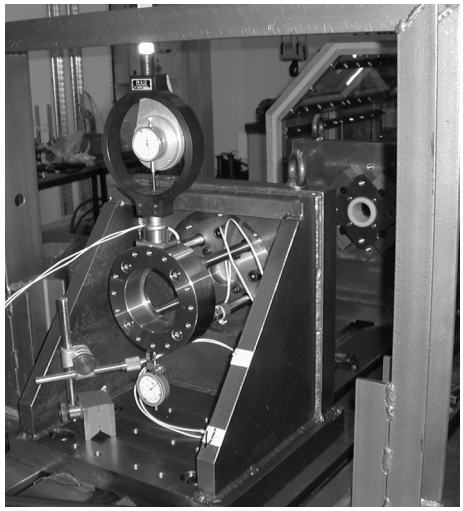

Figure 3: Details of the bearing house and flexible support assembly.

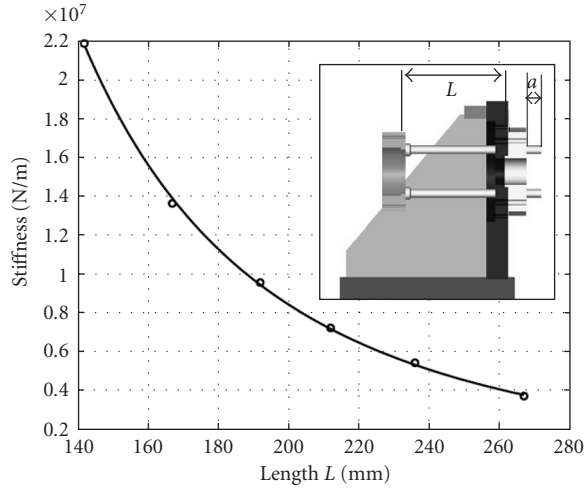


Figure 5: Estimation of the static stiffness versus the length $L$.

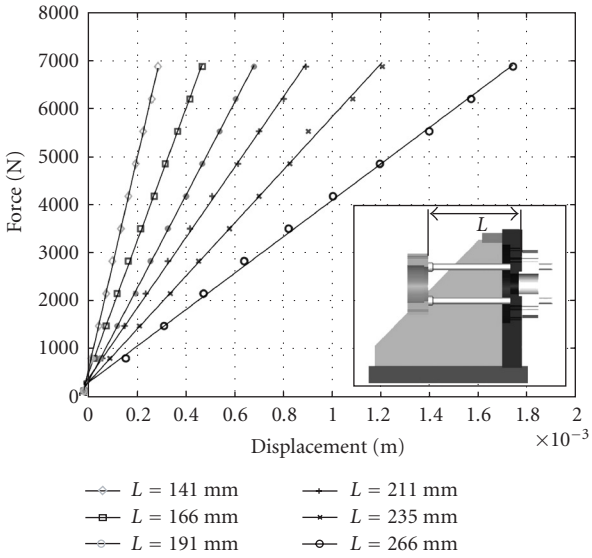


Figure 4: Estimated static stiffness for various lengths of the beams and different static forces.

Moreover, Figure 3 shows details of the bearing housing and flexible support assembly. The support design was based on fourbeams connected to the bearing housing at one end and to a massive block at the other end. Due to the length of these four beams, the support static stiffness in the vertical and horizontal directions varies.

Figure 3 shows the experimental apparatus in order to estimate the various static stiffness versus the length of the beams. The variations of the length of the beams change the bending mode of the four beams, therefore changing the horizontal and vertical stiffnesses of the complete flexible support. This variation of the flexible support will be used in order to increase or decrease the first critical speed of the rotor. Figure 4 shows the estimated static stiffness for various lengths of the beams and different static forces. As illustrated in Figure 5, the support stiffness in the horizontal and vertical directions varies from $3.78 \times 10^6$ N/m for the softest support configuration to $2.2 \times 10^7$ N/m for the stiffest support configuration.

## 3. EXPERIMENTAL PROCEDURE AND RESULTS

The experimental procedure is divided in three parts. Firstly, the Campbelldiagram that gives the evolution of the eigenvalues of the rotor as a function of the rotation speed is established. Secondly, unbalance response of the rotor is undertaken by increasing the speed of the rotor (with a constant acceleration speed profile) until the first critical speed is reached. Finally, the influence of flexible support is studied for three configurations.

### *3.1. The Campbell diagram and the unbalance response*

Firstly, an asynchronous excitation (with a sweep sine approach) that comes from an electromagnetic shaker installed on the bearing support 1 (as illustrated in Figure 6) is used in order to evaluate the frequency response function of several rotating speeds (100 rpm, 500 rpm, 1000 rpm, 1500 rpm, 2000 rpm, 2400 rpm, 2700 rpm, and 3000 rpm). By considering these experimental tests, the Campbell diagram and the evolutions of the first forward and backward whirl modes are built, as illustrated in Figure 7. In this case, the backward whirl modes appears due to the asynchronous excitation given by the electromagnetic shaker. By considering these experimental tests and by interpolating these experimental data, Figure 8 shows the Campbell diagram of the rotor (evolutions of the natural frequenciesas a function of

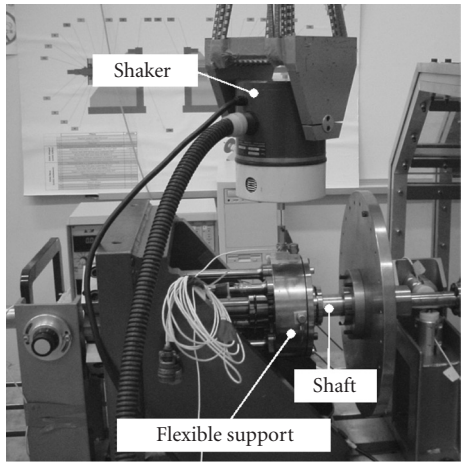


Figure 6: Experimental setup for measuring the Campbell diagram.

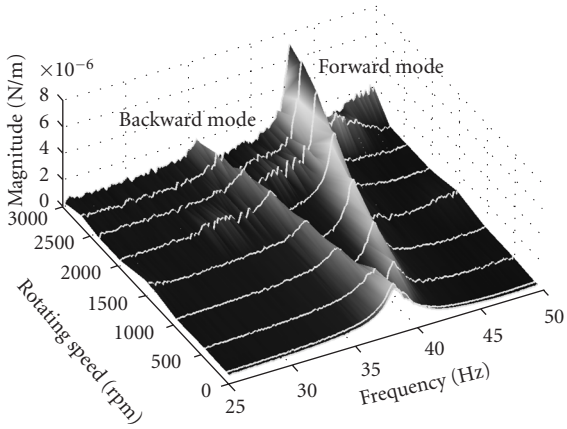


Figure 7: The Campbell diagram and the evolution of the first forward and backward whirl modes.

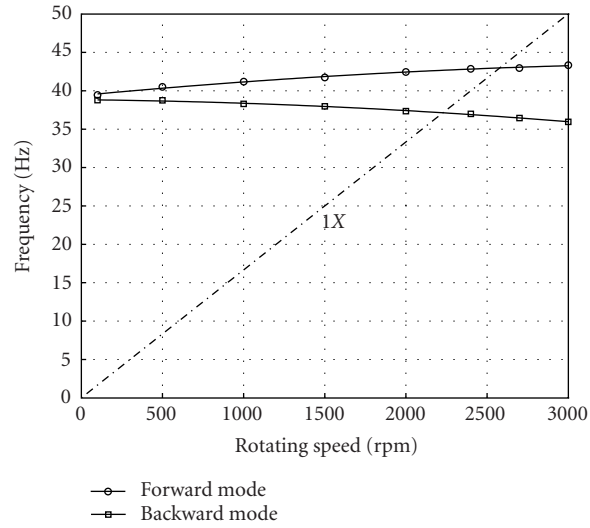


Figure 8: Campbell diagram of the rotor.

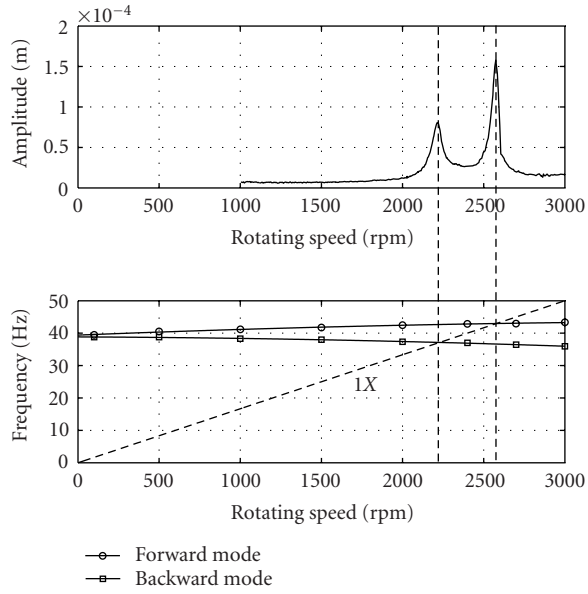


Figure 9: Measured unbalance responses in the horizontal direction at sensor location $B1$. (a) The first response, at 2225 rpm, is the first backward critical speed. (b) The first response, at 2580, is the first forward critical speed.

the rotational speed). As illustrated in Figure 8, the first forward and backward modes start at different values (2225 rpm for the first backward mode and 2580 Hz for the first forward mode) indicating asymmetric properties for the rotor.

The second experimental test consists of an unbalance response of the rotor. In this study, the only goal of this test is to verify experimentally the values of the first forward and backward whirl modes that have been previously obtained by considering the Campbell diagram. Figure 9 shows the measured unbalance responses in the horizontal direction at sensor location $B1$. This figure indicates two responses. The first response, at 2225 rpm, is the first backward critical speed. The second response, at 2580 rpm, is the first forward critical speed.

Then, the value of the first backward and forward critical speeds can be compared by considering the Campbell diagram and the unbalance responses in order to validate the localization of the critical speeds, as illustrated in Figure 9. A perfect correlation between these two experimental tests is obtained. Effectively, the two maximum amplitudes for the unbalance responses (at 2225 rpm for the backward critical speed, and at 2580 rpm for the first forward critical speed) correspond in the Campbell diagram to the intersection of the synchronous excitation line ($1X$ line) with the curves of evolution of the backward and forward modes.

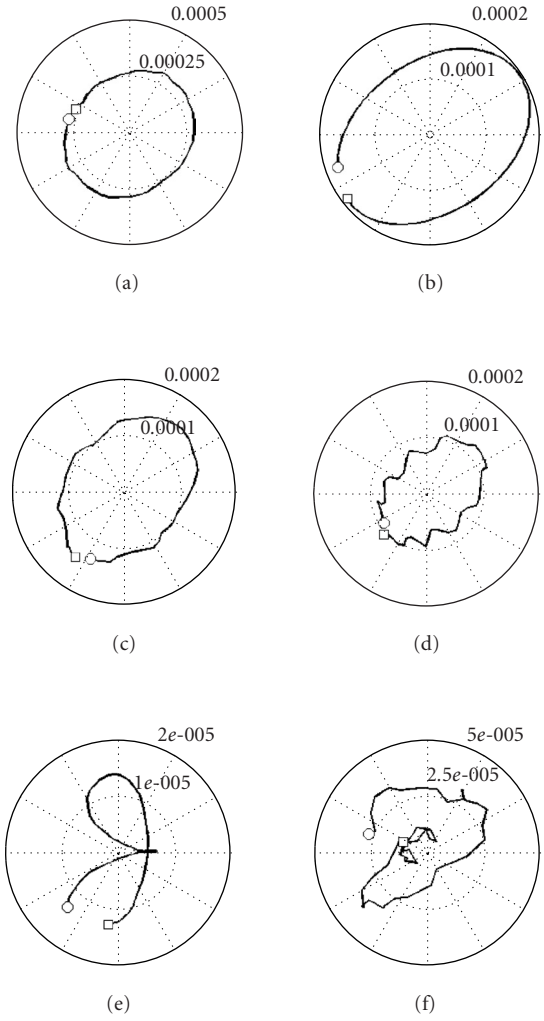


Figure 10: The orbits of the rotor at different measured planes at the first forward critical speed: (a) $A1$, (b) $B1$, (c) $A2$, (d) $A3$, (e) $B2$, and (f) $A4$.

Finally, Figure 10 shows the orbits of the rotor at the different measured planes at the first forward critical speed. Figure 11 shows the deformation of the rotor for the first backward and forward critical speeds by using a cubic interpolation based on the amplitudes obtained for each measured plane. It may be observed that some orbits have an elliptical shape that indicates an asymmetry for the rotor.

### 3.2. Evolution of the flexible support

In this section, the evolution of the first backward and forward critical speeds of the rotor versus the stiffness support will be investigated. The value of this stiffness is modified by varying the length of the four beams of each support, as illustrated in Figure 12. In this study, we consider two new configurations, as indicated in Table 1.

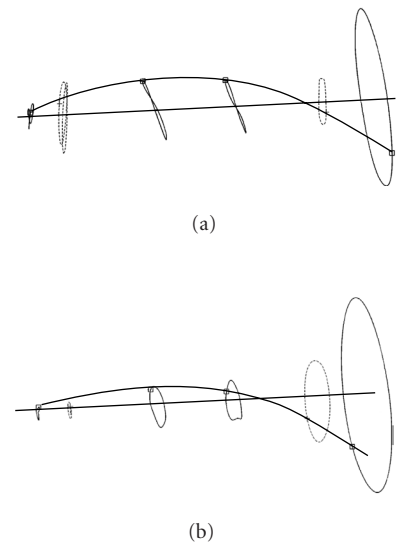


Figure 11: The deformation of the rotor for the first backward and forward critical speeds: (a) backward mode and (b) forward mode.

Table 1: Values of the stiffness support for the three configurations of the experimental rotor.

| Configuration | Stiffness support (N/m) | Length of the beams $L$ (mm) |
|---|---|---|
| Configuration $A$ | $3.78 \times 10^6$ | 266 |
| Configuration $B$ | $5 \times 10^6$ | 240 |
| Configuration $C$ | $7.2 \times 10^6$ | 210 |

Firstly, the Campbell diagram is measured by evaluating FRF of the rotor at several rotating speeds as explained previously. Figures 13 and 14 show the waterfall function for the configuration $B$ and $C$, respectively. In these two cases, the evolution of the first backward and forward modes is clearly identified and the Campbell diagram can be determined as illustrated in Figures 13 and 14, respectively. Then, an unbalance response is performed for each configuration in order to validate the previous measured tests, as shown in Figures 15 and 16. Comparing the three configurations, the first forward critical speed increases within 10.08% and 22.48% for the configurations $B$ and $C$, as indicated in Table 2. The first backward critical speed increases within 3.37% and 8.31% for the configurations $B$ and $C$. This indicates that the support flexibility influences both the backward and forward critical speeds due to the evolution of the bending mode of the four beams constituting the two flexible supports. Moreover, the deformation of the shaft for the three configurations appears to be very similar. The orbits of the rotor for the first critical speed and the associated deformation of the shaft are shown in Figure 17 for the configurations $B$ and $C$.

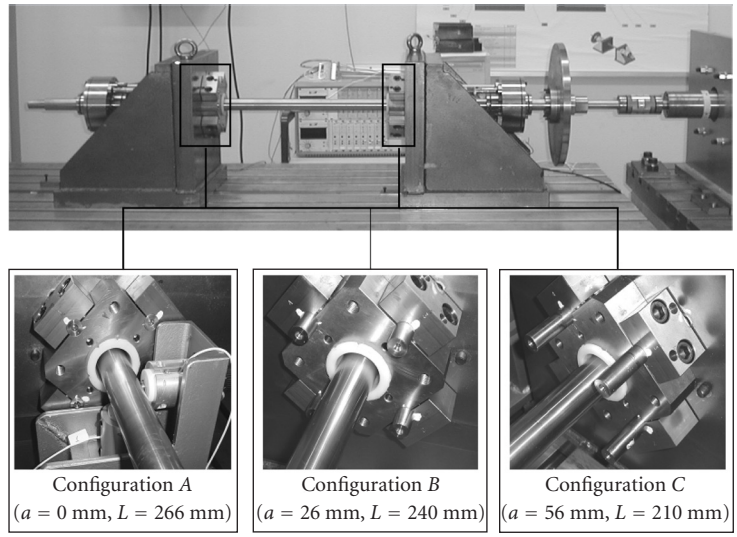


Figure 12: Modified value of the stiffness supports by varying the length of the four beams of each support.

Table 2: Values of the first backward and forward critical speeds of the experimental rotor versus the stiffness support.

| Configuration | First backward critical speed(rpm) | First forward critical speed (rpm) |
|---|---|---|
| Configuration *A* | 2225 | 2580 |
| Configuration *B* | 2300 | 2840 |
| Configuration *C* | 2410 | 3160 |

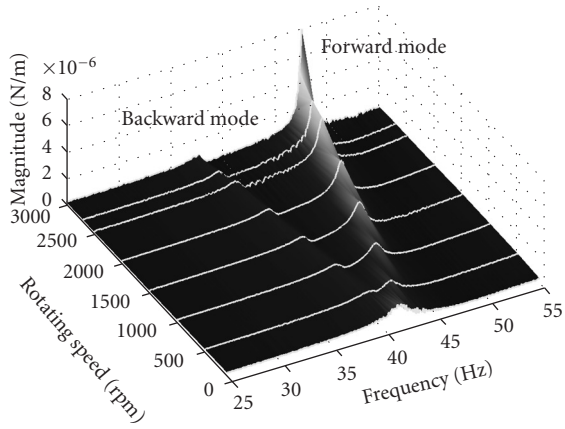


Figure 13: The waterfall function for the configuration *B*.

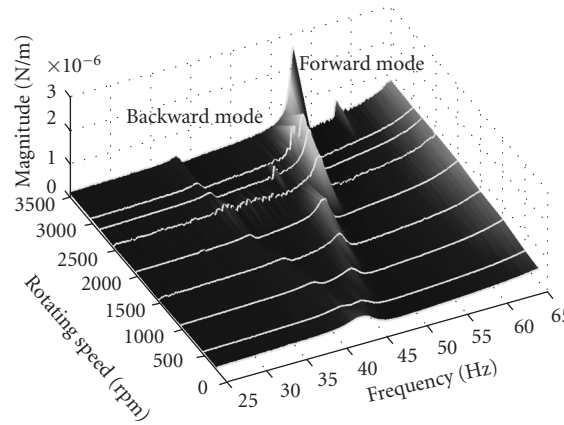


Figure 14: The waterfall function for the configuration *C*.

## 4. NUMERICAL SIMULATIONS

### 4.1. Description of the numerical model

Figure 18 shows the finite element model of the rotor. The shaft is modeled by Timoshenko beam elements with circular cross-sections, discretized in 184 elements containing 185 nodes. Each Timoshenko beam finite element has four degrees of freedoms at each node [17]:

$$(\mathbf{M}_T^b + \mathbf{M}_R^b)\ddot{\mathbf{X}}^b + (\mathbf{C}^b + \Omega\mathbf{G}^b)\dot{\mathbf{X}}^b + \mathbf{K}^b\mathbf{X}^b = \mathbf{0}, \quad (1)$$

where $\mathbf{M}_T^b$ and $\mathbf{M}_R^b$ are the translational and rotary mass matrices of the shaft element. $\mathbf{C}^b$, $\mathbf{G}^b$, and $\mathbf{K}^e$ are the external damping, gyroscopic, and stiffness matrices, respectively. $\Omega$ is the rotational speed and the factor of damping for the shaft. The damping is taken as classical for the sake of simplicity and $\mathbf{C}^b = \beta\mathbf{K}^b$, where the $\beta$ is a constant factor of proportionality, and internal rotor damping has been neglected. The disk is modeled as a rigid disk and given by

$$(\mathbf{M}_T^d + \mathbf{M}_R^d)\ddot{\mathbf{X}}^d + \Omega\mathbf{G}^d\dot{\mathbf{X}}^d = \mathbf{F}^d, \quad (2)$$

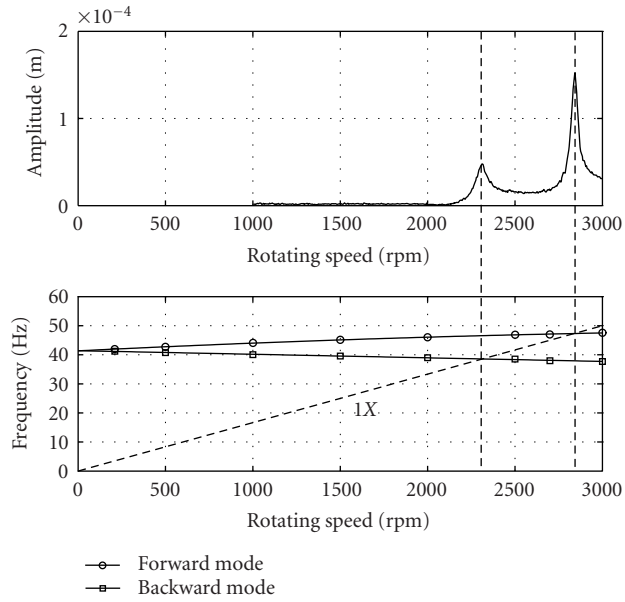


Figure 15: Unbalanced response for configuration *B*.

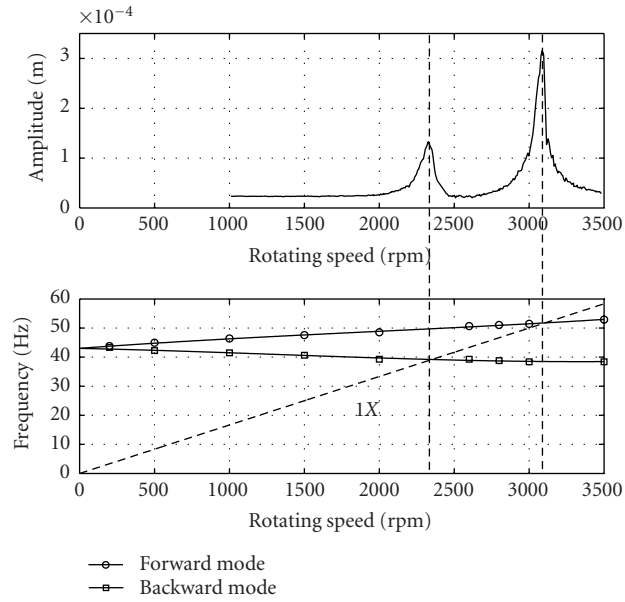


Figure 16: Unbalanced response for configuration *C*.

where $\mathbf{M}_T^d$, $\mathbf{M}_R^d$, and $\mathbf{G}^d$ are the translational mass, rotary mass, and gyroscopic matrices of the disk, respectively. $\mathbf{F}^d$ defines the unbalance forces. The bearings are represented by linear springs and viscous dampers. The rotor is axisymmetrical and the whole system is linear.

Finally, the equations of motion for the complete rotor system is defined as follows:

$$\mathbf{M}\ddot{\mathbf{X}} + (\mathbf{C} + \Omega\mathbf{G})\dot{\mathbf{X}} + \mathbf{K}\mathbf{X} = \mathbf{F}, \tag{3}$$

where $\ddot{\mathbf{X}}$, $\dot{\mathbf{X}}$, and $\mathbf{X}$ are the acceleration, velocity, and displacement vectors. $\mathbf{M}$ is the mass matrix, $\mathbf{C}$ is the damping matrix associated to the nonrotating parts, $\mathbf{G}$ is the gyroscopic matrix, $\mathbf{K}$ is the stiffness matrix, and $\mathbf{F}$ is the unbalance vector. $\Omega$ defines the rotating frequency of the system.

### 4.2. Model updating

The numerical models of the different parts of the rotor are updated according to the modal analysis performed for each component. The comparison between the experimental and numerical modal analyses for the shaft, the shaft and the disk, the uncoupled rotor (corresponding to the shaft, the disk, and the two flexible supports), and the coupled rotor (corresponding to the shaft, the disk, the two flexible supports, and the flexible coupling) is given in Table 3.

Generally speaking, these correlations and procedure should be enough in orderto obtain a available numerical model of the complete rotor. However, some unexpected effects on the dynamical response of the rotor and some difference between the experimental and numerical dynamical tests can be obtained due to the connections between some parts of the rotor during rotational operation. For this study, it is especially the case of the two bearings that interconnect the two flexible supports and the shaft. So it is necessary to perform some additional updating of the complete rotor by considering rotating tests. The design variable that has been chosen in order to correlate the numerical and experimental rotating tests is the moment stiffness of the ball bearing. This design variable is chosen due to the apparition of an angular stiffness that should be observed in the bearing when the shaft bends [19, 20]. Moreover, less information is available for this variable and it has been established that the moment stiffness of the ball bearing induces quite sensible numerical variations for the forward and backward critical speeds of rotors [19, 20].

In order to updatethe finite element model, the correlations between the numerical and experimental tests and the determination of the moment stiffness of the bearing are undertaken by considering physically coherent value for the moment stiffness of the bearing and by the minimization of the following relation:

$$R = \sqrt{\alpha\left(\frac{f_{\text{backward}}^{\text{num}} - f_{\text{backward}}^{\text{exp}}}{f_{\text{backward}}^{\text{exp}}}\right)^2 + \beta\left(\frac{f_{\text{forward}}^{\text{num}} - f_{\text{forward}}^{\text{exp}}}{f_{\text{forward}}^{\text{exp}}}\right)^2 + \chi\left(\frac{V_{\text{backward}}^{\text{num}} - V_{\text{backward}}^{\text{exp}}}{V_{\text{backward}}^{\text{exp}}}\right)^2 + \delta\left(\frac{V_{\text{forward}}^{\text{num}} - V_{\text{forward}}^{\text{exp}}}{V_{\text{forward}}^{\text{exp}}}\right)^2}, \tag{4}$$

Table 3: Experimental and numerical results.

| Element | Mode number | Experimental (Hz) | Numerical (Hz) | Error (%) |
|---|---|---|---|---|
| Shaft | Mode 1 | 69.9 | 70 | 0.14 |
| | Mode 2 | 188.2 | 188.3 | 0.05 |
| | Mode 3 | 359 | 359.9 | 0.25 |
| | Mode 4 | 573.3 | 576.5 | 0.56 |
| Shaft + disk | Mode 1 | 52.9 | 53 | 0.19 |
| | Mode 2 | 128.2 | 128.3 | 0.08 |
| Uncoupled rotor | Mode 1 | 35.5 | 35.8 | 0.72 |
| | Mode 2 | 63 | 64.3 | 2.09 |
| | Mode 3 | 81.5 | 82.1 | 0.7 |
| Coupled rotor | Mode 1 | 40 | 40.5 | 1.25 |
| | Mode 2 | 63 | 64 | 1.59 |

where $f^{\text{num}}_{\text{backward}}$ and $f^{\text{num}}_{\text{forward}}$ are the numerical resonant frequencies of the system at rest for the backward and forward modes, respectively. $f^{\text{exp}}_{\text{backward}}$ and $f^{\text{exp}}_{\text{forward}}$ are the experimental estimated resonant frequencies of the system at rest for the backward and forward modes, respectively. $V^{\text{num}}_{\text{backward}}$ and $V^{\text{num}}_{\text{forward}}$ are the numerical first backward and forward critical speeds of the rotor, and $V^{\text{exp}}_{\text{backward}}$ and $V^{\text{exp}}_{\text{forward}}$ are the experimental first backward and forward critical speeds of the rotor. The coefficients $\alpha$, $\beta$, $\chi$, and $\delta$ allow the variation of the weight of each component of the objective function in order to enhance the participation of a variable in the optimization. In this study $\alpha = \beta = 1$, $\chi = 2$, and $\delta = 3$.

### 4.3. Comparison of the experimental and numerical results for the initial configuration

First of all, the finite element model is correlated by considering the minimization of (4) with the magnitude of the moment stiffness found to be physically coherent. Figure 19 shows the evolution of the residue $R$ for various values of the moment stiffness of the two bearings. Figure 20 illustrates the relative errors between the experimental and numerical values of the backward and forward modes in function of the rotating speed. These relative errors $E_{\text{backward}}$ and $E_{\text{forward}}$ are given for each rotational speed by

$$E_{\text{backward}} = \left| \frac{F^{\text{num}}_{\text{backward}} - F^{\text{exp}}_{\text{backward}}}{F^{\text{exp}}_{\text{backward}}} \right|,$$
$$E_{\text{forward}} = \left| \frac{F^{\text{num}}_{\text{forward}} - F^{\text{exp}}_{\text{forward}}}{F^{\text{exp}}_{\text{forward}}} \right|, \tag{5}$$

where $F^{\text{num}}_{\text{backward}}$ and $F^{\text{exp}}_{\text{backward}}$ define the first numerical and experimental backward mode, respectively. $F^{\text{num}}_{\text{forward}}$ and $F^{\text{exp}}_{\text{forward}}$ define the first numerical and experimental forward mode, respectively.

As shown in Figure 20, the maximum errors $E_{\text{backward}}$ and $E_{\text{forward}}$ observed are less than 3 percentfor all the speed ranges. The predicted first forward critical speed is within 0.4 percent of the first measured forward critical speed and the predicted first backward critical speed is within 1.2 percent ofthe first measured backward critical speed. Finally, the numerical model was updated in order to reproduce the unbalance response of the rotor for the first configuration (configuration $A$). The design variables are the mass of the concentrated unbalance at the disk. The comparisons between the numerical and experimental responses at the two bearing supports are presented in Figure 21.

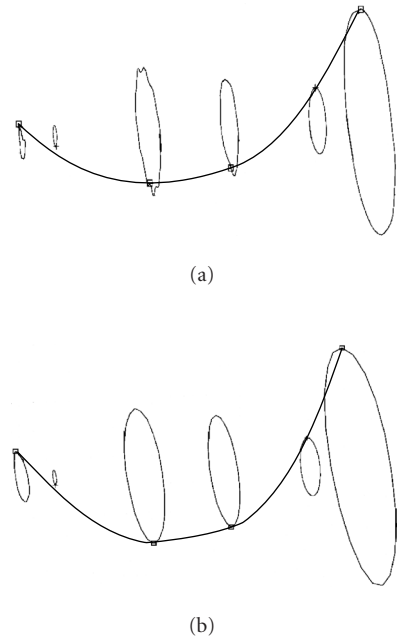

Figure 17: Orbits of the rotor for the first critical speed and the associated deformation of the shaft for (a) configuration $B$ and (b) configuration $C$.

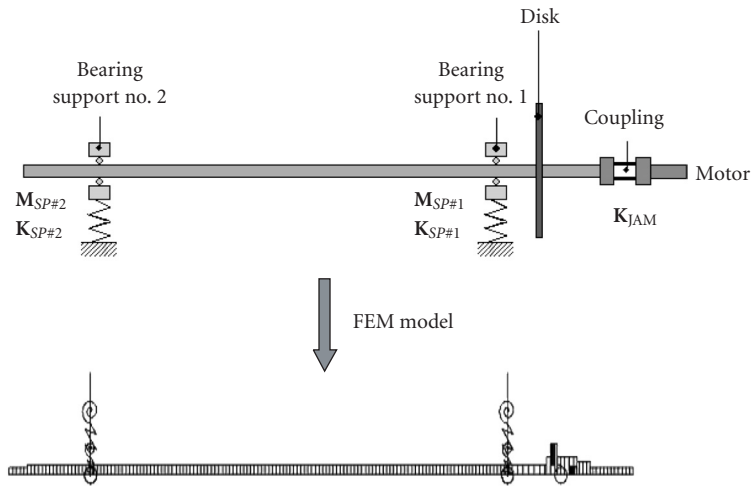


Figure 18: Finite element model of the rotor.

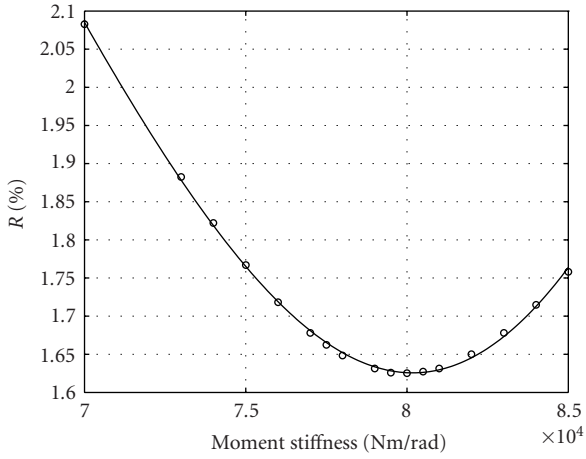


Figure 19: The evolution of the residue $R$ for various values of the moment stiffness of the two bearings.

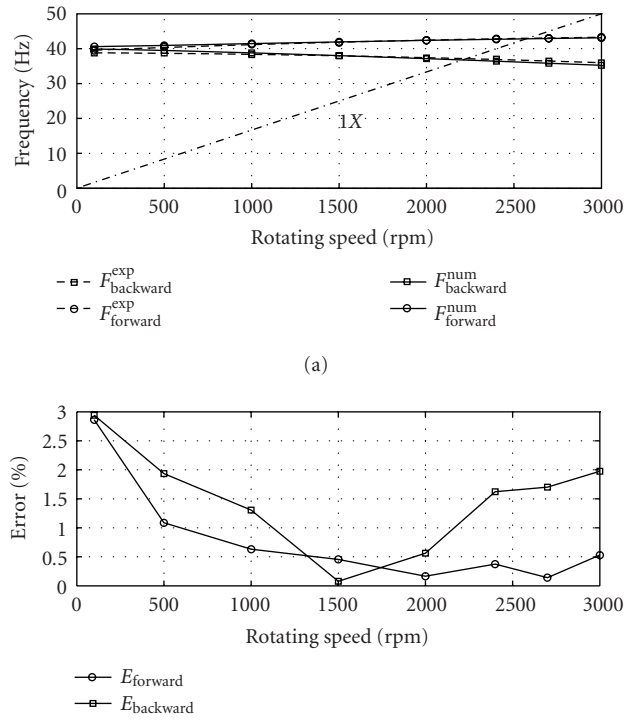


Figure 20: The relative errors between the experimental and numerical values of the backward and forward modes in function of the rotating speed.

### 4.4. Comparison of the experimental and numerical Campbell diagram for various flexible supports

As realized for the initial configuration (configuration $A$), the correlation of the finite element model of the flexible rotor for the second (resp., third) configuration (configuration $B$ (resp., $C$)) is undertaken by considering the minimization of (4) with the magnitude of the moment stiffness. Figures 22 and 23 show the minimization of the moment stiffness of the two bearings. The final values obtained for the numerical model are in physically acceptable for both configuration of the flexible rotor.

Figures 24 and 25 show the relative errors $E_{backward}$ and $E_{forward}$ errors between the experimental and numerical values of the backward and forward modes in function of the rotating speed.

For the second configuration (configuration $B$), the predicted forward and backward frequencies for all the rotational speed is within 3.5 percent of the measured forward and backward frequencies. Moreover,the maximum errors $E_{backward}$ and $E_{forward}$ are less than 2 percent and 1.1 percent at the first backward and forward critical speeds, respectively. In the case of the third configuration (configuration $C$), the predicted forward and backward frequencies for all the rotational speed is within 9 percent of the measured forward and backward frequencies. The maximum errors $E_{backward}$

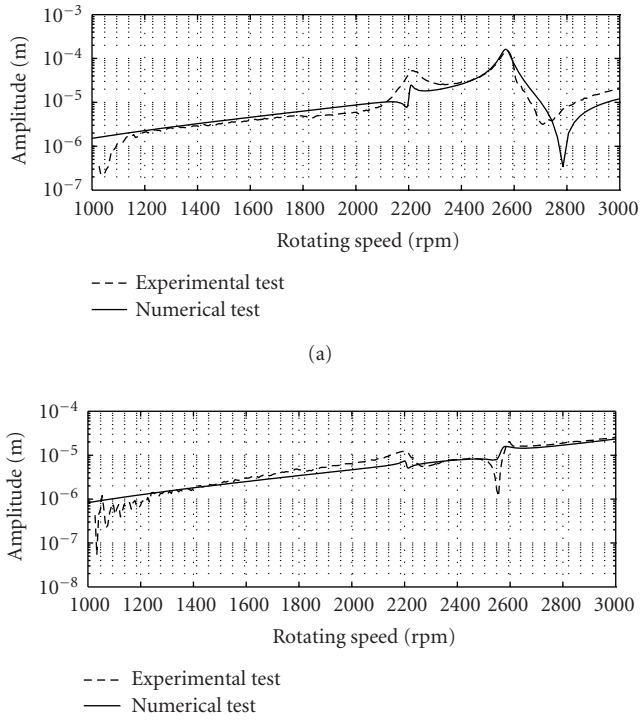


Figure 21: Comparisons between the numerical and experimental responses at the two bearing supports. (a) Bearing support no. 1(plane $B1$). (b) Bearing support no. 2 (plane $B2$).

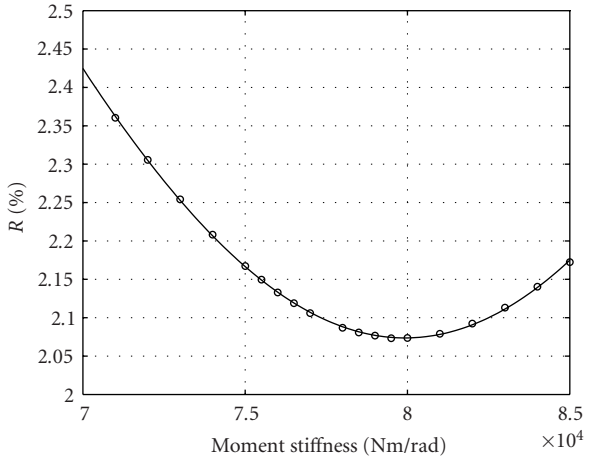


Figure 22: Minimization of the residue $R$ for the configuration $B$.

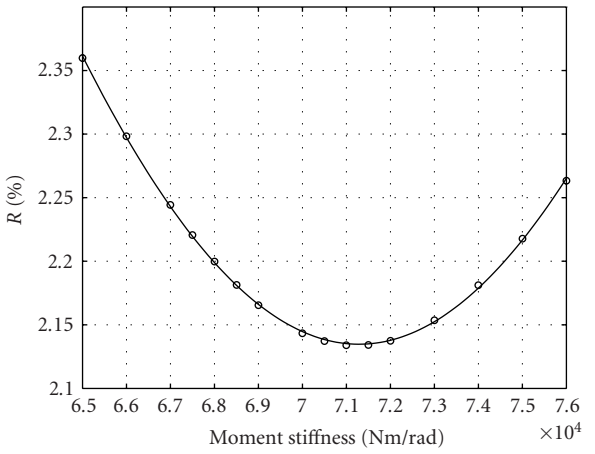


Figure 23: Comparison between the experimental and numerical Campbell diagrams for the configuration $B$.

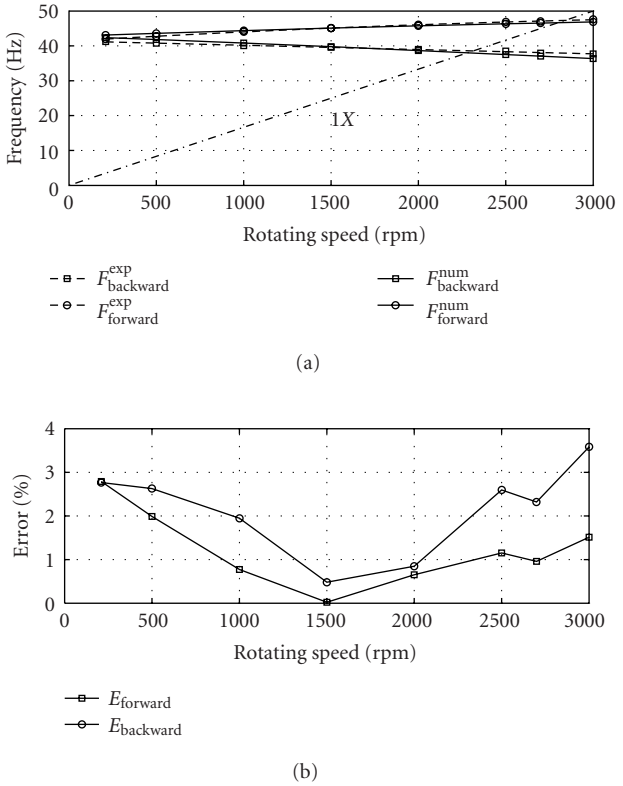


Figure 24: Minimization of the residue $R$ for the configuration $C$.

and $E_{\text{forward}}$ are less than 0.9 percent and 2.2 percent at the first backward and forward critical speeds, respectively.

## 5. CONCLUSION

This research presented a test rig dedicated to the study of rotating machinery. By both an experimental and a numerical approach, the test rig had its dynamics described in detail. The first backward and forward critical speeds were determined experimentally by two methods: the unbalance response and the Campbell diagram.This procedure was applied for three stiffness supports in order to show the effect of the flexibility of the two bearing supports on the first backward and forward critical speeds. In all cases, a perfect correlation for the predicted forward and backward critical speeds was found between the experimental and numerical tests.

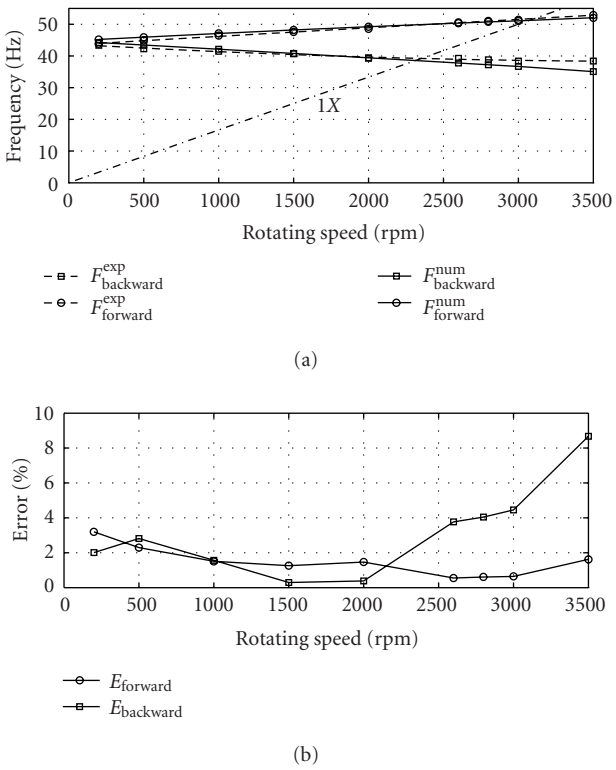


Figure 25: Comparison between the experimental and numerical Campbell diagrams for the configuration *C*.

## REFERENCES


[1] F. F. Ehrich, Ed., *Handbook of Rotordynamics*, McGraw-Hill, New York, NY, USA, 1992.

[2] J. M. Vance, *Rotordynamics of Turbomachinery*, John Wiley & Sons, New York, NY, USA, 1988.

[3] T. Yamamoto and Y. Ishida, *Linear and Nonlinear Rotordynamics: A Modern Treatment with Applications*, John Wiley & Sons, New York, NY, USA, 2001.

[4] D. Childs, *Turbomachinery Rotordynamics: Phenomena, Modeling, and Analysis*, John Wiley & Sons, New York, NY, USA, 1993.

[5] D. E. Bently, C. T. Hatch, and B. Grissom, *Fundamentals of Rotating Machinery Diagnostics*, Bently Pressurized Bearing Press, Minden, Nev, USA, 2002.

[6] S. Edwards, A. W. Lees, and M. I. Friswell, "Experimental identification of excitation and support parameters of a flexible rotor-bearings-foundation system from a single run-down," *Journal of Sound and Vibration*, vol. 232, no. 5, pp. 963–992, 2000.

[7] R. Tiwari and N. S. Vyas, "Non-linear bearing stiffness parameter extraction from random response in flexible rotor-bearing systems," *Journal of Sound and Vibration*, vol. 203, no. 3, pp. 389–408, 1997.

[8] J. K. Dutt and B. C. Nakra, "Dynamics of rotor shaft system on flexible supports with gyroscopic effects," *Mechanics Research Communications*, vol. 22, no. 6, pp. 541–545, 1995.

[9] S. Okamoto, M. Sakata, K. Kimura, and H. Ohnabe, "Vibration analysis of a high speed and light weight rotor system subjected to a pitching or turning motion II: A flexible rotor system on flexible suspensions," *Journal of Sound and Vibration*, vol. 184, no. 5, pp. 887–906, 1995.

[10] J. A. Vázquez, L. E. Barrett, and R. D. Flack, "A flexible rotor on flexible bearing supports: stability and unbalance response," *Journal of Vibration and Acoustics*, vol. 123, no. 2, pp. 137–144, 2001.

[11] A. W. Lees and M. I. Friswell, "The evaluation of rotor imbalance in flexibly mounted machines," *Journal of Sound and Vibration*, vol. 208, no. 5, pp. 671–683, 1997.

[12] J. K. Sinha, A. W. Lees, and M. I. Friswell, "Estimating unbalance and misalignment of a flexible rotating machine from a single run-down," *Journal of Sound and Vibration*, vol. 272, no. 3-5, pp. 967–989, 2004.

[13] A. W. Lees, J. K. Sinha, and M. I. Friswell, "The identification of the unbalance of a flexible rotating machine from a single run-down," *ASME Journal of Engineering for Gas Turbines & Power*, vol. 126, no. 2, pp. 416–421, 2004.

[14] R. Tiwari, A. W. Lees, and M. I. Friswell, "Identification of dynamic bearing parameters: a review," *The Shock and Vibration Digest*, vol. 36, no. 2, pp. 99–124, 2004.

[15] J. K. Sinha, M. I. Friswell, and A. W. Lees, "The identification of the unbalance and the foundation model of a flexible rotating machine from a single run-down," *Mechanical Systems and Signal Processing*, vol. 16, no. 2-3, pp. 255–271, 2002.

[16] R. Tiwari, A. W. Lees, and M. I. Friswell, "Identification of speed-dependent bearing parameters," *Journal of Sound and Vibration*, vol. 254, no. 5, pp. 967–986, 2002.

[17] M. Lalanne, G. Ferraris, and J. Der Hagopian, *Rotordynamics Prediction in Engineering*, John Wiley & Sons, New York, NY, USA, 1990.

[18] H. D. Nelson and J. M. McVaugh, "Dynamics of rotor bearing systems using finite elements," *ASME Journal of Engineering for Industry*, vol. 98, pp. 593–600, 1976.

[19] J. M. De Mul, J. M. Vree, and D. A. Maas, "Equilibrium and associated load distribution in ball and roller bearings loaded in five degrees of freedom while neglecting friction—Part I: general theory and application to ball bearings," *ASME Journal of Tribology*, vol. 111, no. 1, pp. 142–148, 1989.

[20] J. M. De Mul, J. M. Vree, and D. A. Maas, "Equilibrium and associated load distribution in ball and roller bearings loaded in five degrees of freedom while neglecting friction—Part II: application to roller bearings and experimental verification," *ASME Journal of Tribology*, vol. 111, pp. 149–155, 1989.